PHOTONICS Research

Spectrally tunable high-power Yb:fiber chirped-pulse amplifier

Valentina Shumakova,[1,2,*] Vito F. Pecile,[1,3] Jakob Fellinger,[1] Michael Leskowschek,[1] P. E. Collin Aldia,[1,3] Aline S. Mayer,[1] Lukas W. Perner,[1,3] Sarper Salman,[4] Mingqi Fan,[4] Prannay Balla,[4] Stéphane Schilt,[5] Christoph M. Heyl,[4,6,7] Ingmar Hartl,[4] Gil Porat,[8,9] and Oliver H. Heckl[1,10]

[1]*Christian Doppler Laboratory for Mid-IR Spectroscopy and Semiconductor Optics, Faculty Center for Nano Structure Research, Faculty of Physics, University of Vienna, A-1090 Vienna, Austria*
[2]*Photonics Institute, TU Wien, A-1040 Vienna, Austria*
[3]*Vienna Doctoral School in Physics, University of Vienna, A-1090 Vienna, Austria*
[4]*Deutsches Elektronen-Synchrotron DESY, 22607 Hamburg, Germany*
[5]*Laboratoire Temps-Fréquence, Université de Neuchâtel, CH-2000 Neuchâtel, Switzerland*
[6]*GSI Helmholtzzentrum für Schwerionenforschung GmbH, 64291 Darmstadt, Germany*
[7]*Helmholtz-Institute Jena, 07743 Jena, Germany*
[8]*Department of Electrical and Computer Engineering, University of Alberta, Edmonton, Alberta T6G 1H9, Canada*
[9]*Department of Physics, University of Alberta, Edmonton, Alberta T6G 2E1, Canada*
[10]*e-mail: oliver.heckl@univie.ac.at*
Corresponding author: valentina.shumakova@univie.ac.at

Tailoring the properties of the driving laser to the need of applications often requires compromises among laser stability, high peak and average power levels, pulse duration, and spectral bandwidth. For instance, spectroscopy with optical frequency combs in the extreme/visible ultraviolet spectral region requires a high peak power of the near-IR driving laser, and therefore high average power, pulse duration of a few tens of fs, and maximal available spectral bandwidth. Contrarily, the parametric conversion efficiency is higher for pulses with a duration in the 100-fs range due to temporal walk-off and coating limitations. Here we suggest an approach to adjust the spectral characteristics of high-power chirped-pulse amplification (CPA) to the requirements of different nonlinear frequency converters while preserving the low-phase-noise (PN) properties of the system. To achieve spectral tunability, we installed a mechanical spectral shaper in a free-space section of the stretcher of an in-house-developed ytterbium-fiber-based CPA system. The CPA system delivers 100 W of average power at a repetition rate of 132.4 MHz. While gaining control over the spectral properties, we preserve the relative-intensity-noise and PN properties of the system. The high-power CPA can easily be adjusted to deliver either a spectrum ideal for mid-IR light generation (full width at half maximum of ~11 nm, compressed pulse duration of 230 fs) or a spectrum ideal for highly nonlinear processes such as high-harmonic generation (−10 dB level of >50 nm, transform-limited pulse duration of ~65 fs).

1. INTRODUCTION

Yb:fiber laser amplifiers are known for their reliability, stability, simplicity, and scalability to high average and peak powers [1–4]. The fiber geometry and low quantum defect of Yb ions ease the thermal management of the system and allow it to reach hundreds of Watts of average power [5–9]. The development of large-mode-area (LMA) and large-pitch photonic crystal fibers (PCFs) paved the way to high-energy and high-peak-power systems, based on both linear chirped-pulse amplification (CPA) [1,5,10,11] and nonlinear self-similar amplification (SSA) approaches [12–14]. Thus, CPA systems based on a single large-pitch rod-type PCF deliver up to 400 μJ of pulse energy at a 0.5-MHz repetition rate [11], while coherent combining of multiple rod-fiber-based CPAs resulted in mJ pulses and kW-level average power [6,9]. Among the applications of Yb-doped fiber lasers are micromachining and material processing [15], laser-wakefield particle acceleration [16], ranging [17], and various types of spectroscopy. In particular, they

are attractive as femto- and picosecond pump sources for the generation of broadband frequency combs in the extreme/visible ultraviolet (XUV/VUV) [1,18–20], mid-IR [21,22], and THz [23] spectral regions, containing multiple electronic and ro-vibrational transitions. On one hand, generation of broadband coherent XUV/VUV pulses requires high-intensity pump pulses with a duration of the order of tens of fs, and therefore a broad spectrum [24,25]. On the other hand, parametric conversion efficiency from the pump laser frequency to the mid-IR grows with the length of the nonlinear crystals but suffers from a temporal walk-off between ultrashort pulses [21,26,27]. Chirping of the pump pulses to a few hundred fs partially solves the problem, but significantly affects the bandwidth and duration of the frequency-downconverted pulses [28]. Moreover, in some cases, the spectral bandwidth of the pump laser is limited by the availability and costs of dielectric optics [chirped mirrors for optical parametric oscillators (OPOs), diffraction gratings, etc.], as well as by the spectral acceptance of the nonlinear crystals [29,30]. Finally, spectrally tunable pump lasers are of interest for optical parametric chirped pulse amplifiers (OPCPAs), which are often based on sophisticated dispersion management of the seed (signal) pulses leading to wavelength-rigid behavior [31]. Here, changing the pump wavelength by tens of nm can significantly alter the spectrum of the generated idler pulses [32]. Therefore, independent additional control of the pulse duration and the spectral bandwidth of the pump laser is desirable.

The pulse duration of modern CPA and SSA systems is close to its transform-limited value as defined by the spectral bandwidth. The spectral bandwidth is often restricted to several nanometers and hundreds of fs, respectively [11], caused by gain narrowing and apertures of dispersive elements. Using larger-scale diffraction gratings and taking care of the higher orders of dispersion allow for generating pulses with an average power of ∼100 W and a duration of 120–180 fs [1,10,33–35]. Dispersion management based on adjusting the lengths of different types of fibers [35], employing third order compensators [1], or pre-chirping pulses with a combination of gratings and prisms [34] was previously demonstrated. However, the generation of shorter pulses in Yb-based systems requires nonlinear spectral broadening and post- or self-phase compensation, which can be implemented either together with the laser amplification stage [12,14,25,34], or afterwards, using thin plates [36], gas-filled multi-pass cells [37,38], or passive PCFs [39,40]. Systems based on SSA and nonlinear amplification can deliver pulses with a duration of 40–90 fs and a bandwidth of several tens of nm at average powers of 50–100 W. However, working in the nonlinear regime leads to an increased risk of optical damage [25] and coupling of relative intensity noise (RIN) to the fluctuations of the spectral phase and bandwidth, potentially affecting the comb properties of the system. An external nonlinear spectral broadening stage, in turn, also increases the overall noise of the system, as well as its complexity, footprint, and costs [41,42].

Besides the high level of peak and average powers, the generation of frequency combs in all spectral regions via nonlinear processes demands excellent stability of the pump lasers. The characterization of RIN and phase noise (PN) through the

whole amplification system is necessary for the implementation of adequate stabilization. While the RIN of the Yb:fiber CPA is dominated by the RIN of the pump diode of the last amplification stage [43], careful optimization of thermo-optical and optomechanical properties of the system and minimization of the B-integral allow preserving PN properties of the seed laser. Therefore, optimizing the seed laser noise performance is an unavoidable first step in the design of high-power pump systems. For fiber oscillators based on a nonlinear amplifying loop mirror (NALM) and nonlinear polarization evolution (NPE), optimal noise performance can be achieved in the stretched-pulse regime corresponding to close-to-zero, slightly negative net-cavity dispersion [44,45]. A change in the dispersion regime leads to a change in the seed laser spectrum, which influences the spectrum of the consequent CPA stages. Previously, the attempts to correct the seed spectrum were done by mechanically shaping the round-trip gain of the oscillator [46–48], or by inserting a narrowband filter in the cavity [49]. In Refs. [46,47] a mechanical beam block was installed in the free-space section of the NPE and NALM lasers, where the spectrum is spatially dispersed, which was used to spectrally split the round-trip gain of the resonator into two separated regions. This, in turn, resulted in the generation of two independent pulse trains circulating in the cavity with slightly different repetition rates (which can be exploited in dual-comb spectroscopy) and naturally having different net-cavity dispersions. In Ref. [48], an NPE laser operated at large normal group velocity dispersion (GVD), and the mechanical spectral filter was also inserted in a spatially dispersed part of the free-space section of the laser resonator. In this case, the filter blocked the spectral components at the blue edge of the spectrum, which lead to a clipping of the tail of the chirped pulses in the time domain, effectively shortening their duration inside the cavity. That way, operation in a stable mode-locking regime was ensured. However, each filter position required a simultaneous readjustment of the NPE wave plates in the laser cavity. In Ref. [49], the spectrum of the all-normal-dispersion laser was narrowed using a bandpass filter, which led to a certain improvement in the noise properties. However, its performance still cedes to the performance of the NPE/NALM lasers, operating in the stretched-pulse mode-locking regime.

Here, we present a simple technique to obtain spectral tunability for a typical high-power CPA system while preserving the optimal noise performance of the seed laser. Our approach is fast and does not require additional, often time-consuming adjustments of the elements in the seed laser cavity, such as wave plates or a grating pair. The laser system is depicted in detail in Fig. 1 and consists of an oscillator [44], a free-space Martinez-type grating stretcher, a 110-m fiber stretcher, a three-stage fiber-based amplifier, and a grating compressor. Each amplification stage is based on a different type of readily available active fiber, making our results easily applicable to other Yb:fiber-based laser systems.

2. LASER SYSTEM

A. Oscillator and Stretcher

For the oscillator, we chose a design that provides the opportunity to stabilize the repetition rate with a piezo-actuator
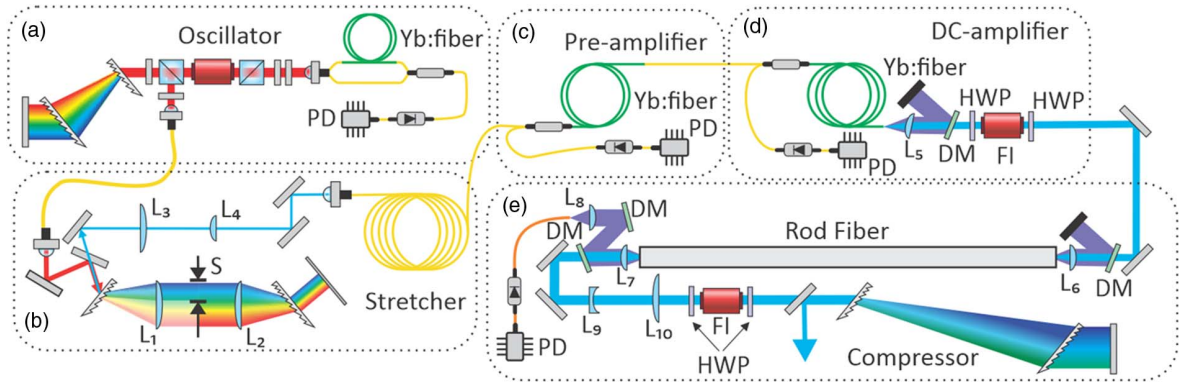
Fig. 1. Scheme of the CPA system: (a) NALM "figure-9" oscillator, having design similar to Ref. [44] and repetition rate of 132.4 MHz; (b) free-space Martinez-type and 110-m fiber stretcher; (c) pre-amplifier; (d) double-clad LMA-based first power amplifier; (e) large-pitch rod-type PCF-based second power amplifier. FI, optical isolator consisting of two crossed polarizers and a Faraday rotator; DM, dichroic mirrors with HR coating for 976 nm and AR for 1030 nm; HWP, half-wave plates; PD, pump diodes; L_1, L_2, identical rectangular-shaped cylindrical lenses with $f = 5$ cm; L_3, L_4, rectangular-shaped cylindrical lenses with $f_3 = 2.54$ cm, $f_4 = 5$ cm; L_5, outcoupling lens, $f = 2.54$ cm; L_6, incoupling lens, $f = 6$ cm; L_7, pump in-coupling and laser out-coupling aspheric lens, $f = 2.6$ cm; L_8, pump collimating aspheric lens, $f = 3.2$ cm; L_9, L_{10}, telescope, $f_9 = -100$ cm, $f_{10} = 300$ cm.

mounted on the cavity end mirror. The design is referred to as a "figure-9" configuration [50] and is based on an all-polarization-maintaining (PM) NALM with a 40-cm-long Yb-doped single-mode PM gain fiber (CorActive-Yb-401-PM), asymmetrically placed in the loop [see Fig. 1(a)]. Based on previous studies [44,45,51], we chose the stretched-pulse operation regime near-zero cavity dispersion, providing the lowest free-running RIN and PN, as well as the narrowest carrier–envelope offset frequency linewidth. In this regime, the oscillator, pumped with ~300 mW power by a fiber-Bragg-grating (FBG) stabilized diode with a central wavelength of 976 nm (Thorlabs BL976-PAG900), produces broadband pulses with a peak at around 1070 nm and a pulse energy of ~200 pJ at the fundamental repetition rate of 132.4 MHz [Fig. 2(c)]. Note that even though the laser repetition rate differs from previous work [44], the general design and mode-locking regime remain similar to Ref. [44].

The pulses were characterized with a second harmonic generation frequency-resolved optical gating (SHG-FROG) apparatus based on a type-1 50-µm-thick BBO crystal. Operating in a close-to-zero slightly negative cavity dispersion regime, the pulse is stretched and compressed at different positions within the cavity. In the case of our laser, the pulse is extracted with a negative chirp and a duration of ~1 ps [Fig. 2(a)]. The oscillator is assembled on a separate breadboard, dispatched from the optical table, and mounted on Sorbothane isolators (vibration absorbing rubber feet) to avoid transfer of mechanical vibrations and acoustic noise from the environment to the seed laser. To avoid nonlinearities and prevent beam-pointing instabilities, we used a short out-coupling fiber ($L \approx 0.2$ m, Thorlabs PM-980) and inverted the sign of the chirp of the laser pulses in a free-space stretcher. The stretcher has a Martinez configuration and consists of two transmission diffraction gratings (T-1600-1030s, LightSmyth Technologies), two cylindrical lenses with $f_{1,2} = 50$ mm, and a silver mirror retroreflector [Fig. 1(b)]. The pulses before the stretcher have a pulse duration of ~800 fs, a negative chirp, and a power of
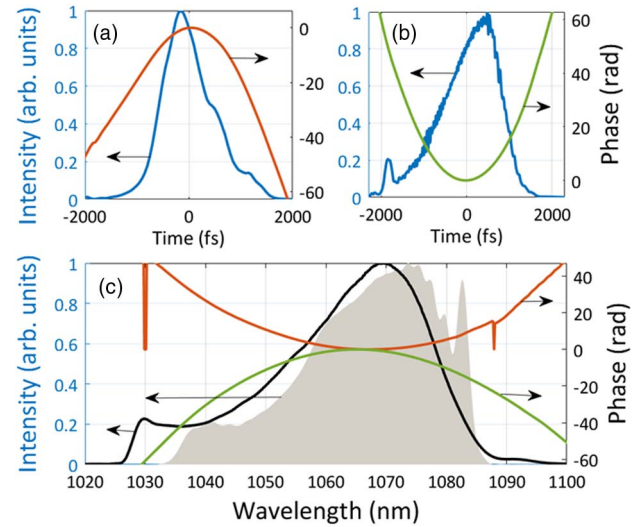

Fig. 2. Spectral–temporal characterization of the pulse from the oscillator and after free-space stretcher. (a), (b) Temporal envelope and phase retrieved from the SHG-FROG traces. (c) Spectrum measured with AQ6315A Ando Yokogawa spectrometer (solid black line) and retrieved from SHG-FROG traces (shaded gray area); the solid orange lines in (a) and (c) correspond to the phase from the oscillator (retrived from FROG), and the solid green lines in (b) and (c) to the pulses after the stretcher.

25 mW (180 pJ); the pulses after the stretcher have a positive chirp, a duration of ~1.5 ps at FWHM and ~3 ps at the rms (root-mean-square) level [Fig. 2(b)], and a power of ~15 mW (108 pJ). After the stretcher, we inserted a cylindrical lens telescope ($f_3 = 25.5$ mm, $f_4 = 50$ mm) to compensate for beam astigmatism, and a collimator to couple the pulses to the fiber stretcher and the first two amplification stages. The fiber stretcher consists of ~110 m fiber (Thorlabs PM-980) and stretches the pulses to ~110 ps duration at the rms level [Figs. 3(c) and 3(e)].
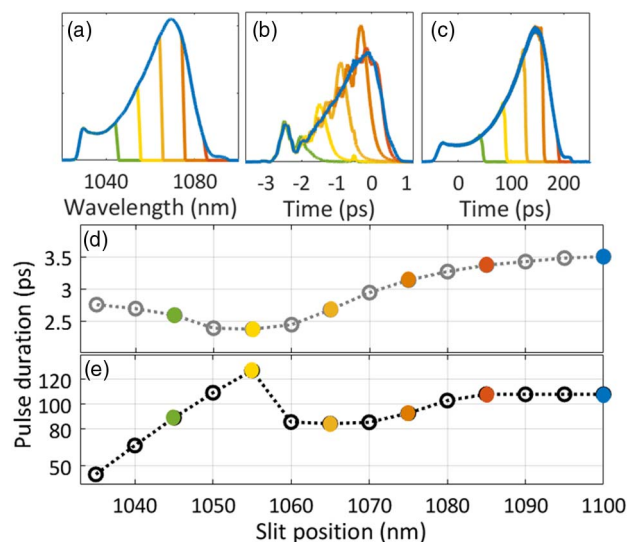
Fig. 3.   (a) Spectra after the slit-type aperture; (b), (c) calculated IFFT pulse shape after free-space (b) and fiber stretchers (c) at different widths of the slit-type aperture; the spectra were numerically smoothened for easier readability. (d), (e) Seed pulse duration at rms level after free-space (d) and the 110-m fiber stretchers (e) in dependence of the cutoff of the spectral red wing.

B. Spectral Filter

To achieve spectral tunability, we installed a slit-type aperture into the imaging plane between lenses L_1 and L_2 of the free-space stretcher [Fig. 1(b)], where the spectrum is spatially dispersed and the beam is collimated. It allows us to control the spectral width by changing the opening of the slit. Note that, similar to the case of a high-energy low-repetition-rate CPA [52], the shape and the position of the mechanical element can be chosen arbitrarily, which allows us to tailor the seed spectrum to a particular task (such as, shifting the central wavelength to avoid gain narrowing). Simultaneous to changing the spectrum, we act on the temporal shape and duration of the pulse. To estimate this influence, we mapped the spectral domain into the temporal domain by performing an inversed fast Fourier transformation (IFFT) on the cropped spectra [Fig. 3(a)] with the calculated group delay dispersion (GDD) and third order dispersion (TOD) of the fiber stretcher and the phase retrieved from the FROG traces, as measured after the free-space stretcher [Figs. 2(b) and 2(c)]. The results are presented in Fig. 3 and show that cutting spectral components in the low-intensity tail after 1080 nm does not significantly influence the pulse duration. Further closing the aperture and corresponding to a wavelength cutoff of 1065 nm leads to a linear decrease of the rms-level pulse duration to ~80 ps after the fiber stretcher and ~2.4 ps after the free-space stretcher, respectively [Figs. 3(a) and 3(b)]. Afterwards, a change in the pulse shape occurs [a double peak appears instead of the single one, as shown with the light yellow line in Figs. 3(c) and 3(d)]. It results in an artificial "elongation" of the pulse duration after the fiber stretcher to ~120 ps. However, with further narrowing of the spectral bandwidth, the duration again linearly decreases to ~50 ps if the red wing of the spectrum is cut at ~1035 nm. In our work, we decided to limit the

cut wavelength to ~1045 nm, where the pulse duration after the fiber stretcher is ~90 ps.

C. Amplification Chain

The amplifier system consists of three stages: (i) low-power pre-amplifier [Fig. 1(c)]; (ii) first power amplifier based on a flexible double-clad LMA fiber [Fig. 1(d)]; (iii) second power amplifier based on a rod-type large-pitch PCF with distributed mode filter design [Fig. 1(e)] [53,54]. The first two amplification stages have an all-fiber design and are spliced directly to the output of the fiber stretcher.

The pre-amplifier stage is based on a Yb-doped single-clad PM gain fiber (YB 401-PM, CorActive High-Tech, Inc., length of 0.5 m) and pumped by an FBG-stabilized laser diode at 976 nm (Thorlabs BL976-PAG700). The pump is delivered to the active fiber using a PM filter wavelength division multiplexer (PMFWDM, Advanced Fiber Resources, Ltd.).

The active element in the second stage is a 2-m-long double-clad fiber (Yb1200-10/125DC-PM, nLight), pumped by a 20-W conduction-cooled fiber-coupled diode laser module at 976 nm, which is connected to the active fiber via a PM pump and signal combiner (PMMPC, Advanced Fiber Resources, Ltd.). The output tip of the double-clad fiber is angularly cleaved (8°) to prevent amplification of the Fresnel backreflection. The tip is placed on an *XYZ* translation stage, and the amplified laser light is outcoupled from the fiber with an $f = 25.4$ mm lens, tilted to compensate for the effect of the angular cleavage. The residual unabsorbed pump is filtered out using a dichroic mirror.

After passing through a half-wave plate (HWP) and a Faraday isolator, a beam with a diameter of ~2.3 mm (measured at the position of the coupling lens) is focused by an $f = 60$ mm lens on the input facet of the rod-type large-pitch PCF (aeroGAIN-ROD module, NKT Photonics Inc.) with a mode diameter of ~55 μm and a length of 80 cm. Here, we purposely avoided building the 4-f imaging system between the two fiber amplifiers to reduce the influence of higher-order modes. The rod fiber is backside-pumped (to minimize non-linear phase accumulation) by a 240-W conduction-cooled fiber-coupled laser diode at 976 nm (DILAS Diodenlaser GmbH). The pump light is delivered from the diode by a 200-μm step-index multimode fiber with a numerical aperture of 0.22 and collimated by an aspheric $f = 32$ mm lens. The residual pump is partially dumped on a water-cooled annular beam block before the seed-coupling lens [1]; the rest is filtered out by a dichroic mirror before the input facet of the rod fiber and dumped on another water-cooled beam stopper. The polarization of the seed light launched into the rod fiber is aligned with the birefringent axes by another HWP. After the rod fiber, the beam goes through an aspheric lens with a focal distance of $f = 26$ mm, optimized for pump coupling, and through a beam expander, consisting of two lenses with focal distances of $f = -100$ mm and $f = 300$ mm. After the telescope, there is an HWP and a Faraday isolator. The pulses are recompressed in a grating compressor, consisting of two diffraction gratings (T-1600-1030s Series, LightSmyth Technologies) with a groove density of 1600 lines/mm, working in transmission, and optimized for 1030 nm central wavelength at 55.5° angle of incidence (transmissivity of ~95% for

the first order diffracted light). Another HWP is installed in front of the compressor to maximize the power throughput.

3. RESULTS

A. CPA Performance and Spectral Tuning

Having a broadband seed spectrum with a center of gravity outside of the amplification maximum of the Yb gain allows us to generate broadband spectra with ~50 nm bandwidth at 10% from the maximum level after each amplification stage, supporting ~65 fs Fourier transform-limited pulse duration [Figs. 4(c)–4(e)]. The power levels achieved at each stage are around 0.35 W, 9 W, and 100 W ($E \approx 0.75$ μJ) at the corresponding pump powers of 0.78 W, 18.5 W, and 180 W [Figs. 4(a) and 4(b)] and conversion efficiencies of 45%, 47%, and 54%, respectively. The spectral bandwidth of the 100 W CPA system reported here is comparable with state-of-the-art fiber-based SSAs, where spectral dynamics is governed by nonlinear processes such as self-phase modulation (SPM), self-steepening, and stimulated Raman scattering (SRS) [25,34]. However, in contrast to the nonlinearly broadened spectra of SSA schemes [12,13,25], the spectrum from CPA systems is smooth and does not exhibit interferences, which are typical for SPM and SRS [Figs. 4(c)–4(e)].

We measured the spectra, power, and beam profiles after each power amplification stage (Fig. 4), as well as the spectra after the pre-amplifier, at different widths of the slit aperture in the stretcher. These different widths correspond to different seed spectra (see also Fig. 3). We did not notice a significant difference in the conversion efficiency of the double-clad-fiber amplifier. For the rod-fiber amplifier, the maximum conversion efficiency of 56% was achieved at the narrowest seed spectra,
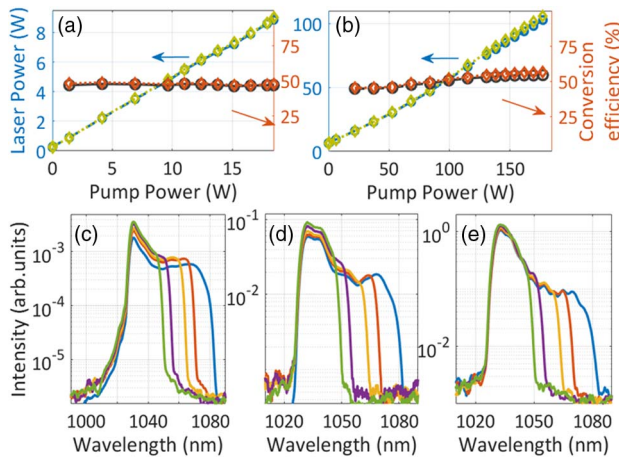
since it falls into the maximum of the Yb-gain curve and the rod fiber itself is optimized for the 1030–1040 nm spectral region.

After the rod fiber, the beam was expanded to a diameter of ~3 mm and collimated with a two-lens telescope ($f_1 = $ −100 mm, $f_2 = 300$ mm), and passed through an HWP, a thin film polarizer, and a metal iris, to filter out the residual light from the cladding and to clean the polarization. The spectrally narrowed pulses were recompressed in the grating compressor and characterized with an SHG–FROG apparatus. The pulses have a duration of ~230 fs and a smooth temporal envelope, containing ~90% of the power under the main peak (see Fig. 5). The transmissivity of the compressor is ~74%, which results in a peak power of 2.2 MW.

B. Noise Measurements and Analysis

We have examined the PN properties of the system using a signal source analyzer (Rohde&Schwarz FSWP-8) with a frequency range from 1 MHz to 8 GHz and an InGaAs photodiode (Thorlabs DET08CL) with 5 GHz bandwidth, connected to the signal source analyzer via a 50-Ω RF terminator where necessary. The measurements were performed in a highly attenuated tightly focused beam to prevent detector saturation. The PN was characterized using the 15th harmonic of the laser repetition rate as the carrier frequency and renormalized afterwards to the laser repetition rate [55]. The measurements were performed in a single-sideband mode with 2000 cross-correlations. For each frequency segment, the resolution bandwidth factor was 1% [55].

The RIN measurement was performed as a baseband measurement using the same signal source analyzer and a Si detector (Thorlabs PDA36A-EC) with a bandwidth of 10 MHz ($f_{3\,dB}$), 200 cross-correlations, a sufficiently small mode, and a resolution bandwidth factor of 1% for each frequency segment as above.

We compared the PN and RIN of the oscillator (black curves in Fig. 6) and of the amplifier after the grating compressor with (blue curves in Fig. 6) and without (green curves in Fig. 6) the slit-type aperture in the free-space stretcher. The PN of the oscillator is preserved in the CPA for Fourier frequencies up to 200 kHz, after which minor deviations (<5 dB) are observed [Fig. 6(b)]. At the same time, the RIN of the system differs significantly from the oscillator and, as expected, is defined mainly by the RIN of the pump diode of the final

Fig. 4. Power slopes of the double-clad-based second stage amplifier (a) and the rod-fiber-based third stage amplifier (b) seeded by different spectra [blue circles correspond to a fully opened slit aperture in the stretcher and the broadest seed spectra, green diamonds to the narrowest spectrum in (c)–(e) and the narrowest seed spectra]. Spectra with (orange line) and without (blue line) spectral filter (slit) inserted in the free-space stretcher after: (c) preamplifier (P_{out} = 300 mW); (d) first power amplifier (P_{out} = 9 W); (e) second power amplifier (P_{out} = 100 W) normalized on the integral area under the curve. Spectra are measured with an AQ6315A Ando Yokogawa spectrometer. Note the logarithmic intensity scale.
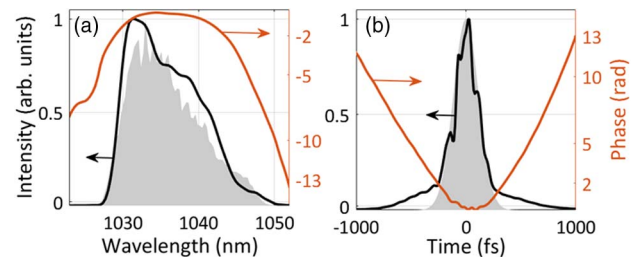

Fig. 5. (a) Spectral intensity and phase, as well as (b) temporal envelope and phase of 100-W pulses retrieved from SHG-FROG traces. Filled gray areas correspond to the spectrum of the 100-W pulses measured with an AQ6315A Ando Yokogawa spectrometer (a) and to a calculated Gaussian pulse with the same duration as the duration of the retrived pulse from the FROG trace (230 fs) (b).
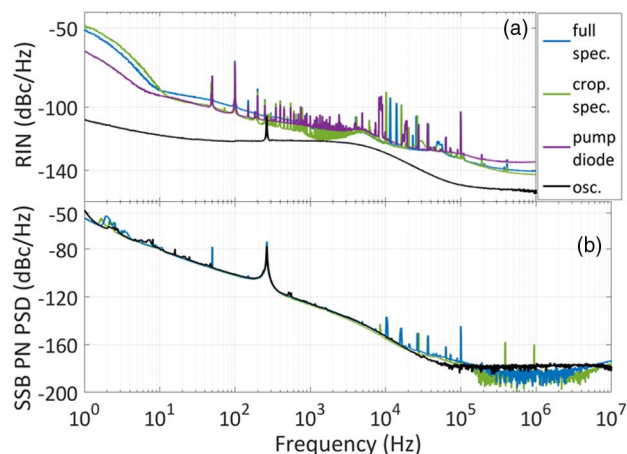
Fig. 6. (a) RIN and (b) single sideband (SSB) PN power spectral density (PSD) measured for the oscillator (black line); broadest (blue line) and narrowest (green line) seed pulses after amplification to 100 W, and the pump diode of the last amplification stage (purple line).

amplification stage up to 50 kHz [Fig. 6(a), purple curve] [43]. The pump RIN is coupled to the amplifier via fluctuations of the population of the upper level, which take place at the frequencies below the corner frequency [56]. Note that the narrow spikes in the PN and RIN spectra originate from high-voltage electronics, required for the operation of power amplification stages. We attribute a common peak located at ~290 Hz in the noise power spectral density (PSD) to the relaxation oscillation of the seed-laser resonator [44,45].

In particular, we could show excellent preservation of the oscillator PN over the full range of investigated Fourier frequencies. The preservation of the PN properties points towards the absence of amplitude-to-PN coupling. No additional B-integral was accumulated, even when the spectrum was cropped and the pulse duration after the fiber stretcher was correspondingly shortened. Moreover, the mechanical spectral filter placed outside of the laser cavity does not introduce mechanical or acoustic noise above a Fourier frequency of 1 Hz.

4. CONCLUSION

We demonstrated a three-stage 100 W Yb:fiber CPA system, which allows tailoring the spectrum of the amplified pulses to a particular application while preserving the low PN of the seed laser. Our seed laser was optimized for low-noise operation and worked in the stretched-pulse regime with close-to-zero slightly negative net-cavity dispersion. The chosen state of operation provided enough power to saturate the amplification chain.

The RIN performance of our system is limited by the last amplification stage pump diode and comparable with state-of-the-art high-average-power fiber-based amplifiers seeded by free-running oscillators [1]. When compared with an SSA-based high-power system, having similar maximum spectral bandwidth [12], we do not observe degeneration of the PN with increasing output power. To preserve the PN, we ensured that the system was thermally and mechanically stable, and operating in a linear CPA regime. Specifically, we:

(i) inverted the sign of the seed pulse chirp to avoid an accumulation of B-integral and amplitude-to-PN coupling in the fiber stretcher;
(ii) ensured that the length of the fiber stretcher was sufficient to stretch pulses to >80 ps duration to avoid nonlinear effects in the subsequent amplification chain at all desired spectral bandwidths;
(iii) detached the oscillator from the optical table, by setting it on a separate breadboard placed on damping rubber feet, and used a short out-coupling fiber (not introducing nonlinearities due to the low light intensity and short propagation path) to guide the pulses to the stretcher.

The system delivers 100-W pulses at a repetition rate of 132.4 MHz, which corresponds to a pulse energy of 0.75 μJ. The widths of the spectra of the amplified pulses can be tuned by adjusting the micrometer screw of a slit-type aperture placed in the imaging plane of a Martinez-type stretcher. The broadest amplified spectrum spreads from 1025 nm to 1080 nm and supports a Fourier transform-limited pulse duration of 65 fs, which is comparable to state-of-the-art nonlinear amplifiers [25,34]. Such a spectrum is supported by each amplification stage, based on three different popular types of active Yb:fibers, making the method suitable for various CPA configurations. In contrast, cropping the seed spectrum allows confining the spectral density between 1025 nm and 1045 nm, where inexpensive, high-quality optical coatings, and many off-the-shelf optical components are available. The compressed narrowband pulses have a duration of 230 fs, which is only 13% longer than the Fourier-limited pulse duration of 200 fs calculated for the cropped spectrum. A peak power of 2 MW and a duration of 230 fs are well suited as a pump for high-efficiency OPOs and difference-frequency-generation stages [21]. The here-presented spectral filter installed in the Martinez stretcher does not affect the noise performance of the system, in contrast to spectral filters installed directly in the laser cavity [48,49]. Moreover, the shape of the filter can be chosen arbitrarily: not only to crop the spectrum but also, for instance, to prevent spectral gain narrowing [52].

Disclosures. The authors declare no conflicts of interest.

Data Availability. Data underlying the results presented in this paper are not publicly available at this time but may be obtained from the authors upon reasonable request.

REFERENCES

1. X. Li, M. A. R. Reber, C. Corder, Y. Chen, P. Zhao, and T. K. Allison, "High-power ultrafast Yb:fiber laser frequency combs using commercially available components and basic fiber tools," Rev. Sci. Instrum. **87**, 093114 (2016).
2. G. Chang and Z. Wei, "Ultrafast fiber lasers: an expanding versatile toolbox," iScience **23**, 101101 (2020).

3. D. J. Richardson, J. Nilsson, and W. A. Clarkson, "High power fiber lasers: current status and future perspectives [Invited]," J. Opt. Soc. Am. B **27**, B63–B92 (2010).

4. C. Jauregui, J. Limpert, and A. Tünnermann, "High-power fibre lasers," Nat. Photonics **7**, 861–867 (2013).

5. D. Luo, Y. Liu, C. Gu, Z. Zhu, Z. Deng, L. Zhou, Y. Di, G. Xie, and W. Li, "130 W, 180 fs ultrafast Yb-doped fiber frequency comb based on chirped-pulse fiber amplification," Opt. Express **28**, 4817–4824 (2020).

6. A. Klenke, S. Breitkopf, M. Kienel, T. Gottschall, T. Eidam, S. Hädrich, J. Rothhardt, J. Limpert, and A. Tünnermann, "530 W, 13 mJ, four-channel coherently combined femtosecond fiber chirped-pulse amplification system," Opt. Lett. **38**, 2283–2285 (2013).

7. T. Eidam, S. Hanf, T. V. Andersen, E. Seise, C. Wirth, T. Schreiber, T. Gabler, J. Limpert, and A. Tünnermann, "Femtosecond fiber CPA system emitting 830 W average output power," Opt. Lett. **35**, 94–96 (2010).

8. P. Ma, R. Tao, L. Huang, X. Wang, P. Zhou, and Z. Liu, "608 W average power picosecond all fiber polarization-maintained amplifier with narrow-band and near-diffraction-limited beam quality," J. Opt. **17**, 075501 (2015).

9. E. Shestaev, S. Hädrich, N. Walther, T. Eidam, A. Klenke, I. Seres, Z. Bengery, P. Jójárt, Z. Várallyay, Á. Börzsönyi, and J. Limpert, "Carrier-envelope offset stable, coherently combined ytterbium-doped fiber CPA delivering 1 kW of average power," Opt. Lett. **45**, 6350–6353 (2020).

10. H. Chang, Z. Cheng, R. Sun, Z. Peng, M. Yu, Y. You, M. Wang, and P. Wang, "172-fs, 27-μJ, Yb-doped all-fiber-integrated chirped pulse amplification system based on parabolic evolution by passive spectral amplitude shaping," Opt. Express **27**, 34103–34112 (2019).

11. C. P. K. Manchee, J. Möller, and R. J. D. Miller, "Highly stable, 100 W average power from fiber-based ultrafast laser system at 1030 nm based on single-pass photonic-crystal rod amplifier," Opt. Commun. **437**, 6–10 (2019).

12. D. Luo, Y. Liu, C. Gu, C. Wang, Z. Zhu, W. Zhang, Z. Deng, L. Zhou, W. Li, and H. Zeng, "High-power Yb-fiber comb based on pre-chirped-management self-similar amplification," Appl. Phys. Lett. **112**, 061106 (2018).

13. Y. Liu, W. Li, J. Zhao, D. Bai, D. Luo, and H. Zeng, "High-power pre-chirp managed amplification of femtosecond pulses at high repetition rates," Laser Phys. Lett. **12**, 075101 (2015).

14. J. Zhao, W. Li, C. Wang, Y. Liu, and H. Zeng, "Pre-chirping management of a self-similar Yb-fiber amplifier towards 80 W average power with sub-40 fs pulse generation," Opt. Express **22**, 32214–32219 (2014).

15. Z. Bai, Z. Bai, X. Sun, Y. Liang, K. Wang, D. Jin, and Z. Fan, "A 33.2 W high beam quality chirped-pulse amplification-based femtosecond laser for industrial processing," Materials **13**, 2841 (2020).

16. F. Albert, M. E. Couprie, A. Debus, M. C. Downer, J. Faure, A. Flacco, L. A. Gizzi, T. Grismayer, A. Huebl, C. Joshi, M. Labat, W. P. Leemans, A. R. Maier, S. P. D. Mangles, P. Mason, F. Mathieu, P. Muggli, M. Nishiuchi, J. Osterhoff, P. P. Rajeev, U. Schramm, J. Schreiber, A. G. R. Thomas, J. L. Vay, M. Vranic, and K. Zeil, "2020 roadmap on plasma accelerators," New J. Phys. **23**, 031101 (2021).

17. J. Fellinger, G. Winkler, P. E. C. Aldia, A. S. Mayer, V. Shumakova, L. W. Perner, V. F. Pecile, T. Martynkien, P. Mergo, G. Soboń, and O. H. Heckl, "Simple approach for extending the ambiguity-free range of dual-comb ranging," Opt. Lett. **46**, 3677–3680 (2021).

18. J. Boullet, Y. Zaouter, J. Limpert, S. Petit, Y. Mairesse, B. Fabre, J. Higuet, E. Mével, E. Constant, and E. Cormier, "High-order harmonic generation at a megahertz-level repetition rate directly driven by an ytterbium-doped-fiber chirped-pulse amplification system," Opt. Lett. **34**, 1489–1491 (2009).

19. S. Stellmer, G. Kazakov, M. Schreitl, H. Kaser, M. Kolbe, and T. Schumm, "Attempt to optically excite the nuclear isomer in 229Th," Phys. Rev. A **97**, 062506 (2018).

20. I. Pupeza, C. Zhang, M. Högner, and J. Ye, "Extreme-ultraviolet frequency combs for precision metrology and attosecond science," Nat. Photonics **15**, 175–186 (2021).

21. K. Iwakuni, G. Porat, T. Q. Bui, B. J. Bjork, S. B. Schoun, O. H. Heckl, M. E. Fermann, and J. Ye, "Phase-stabilized 100 mW frequency comb near 10 μm," Appl. Phys. B **124**, 128 (2018).

22. F. Adler, K. C. Cossel, M. J. Thorpe, I. Hartl, M. E. Fermann, and J. Ye, "Phase-stabilized, 1.5 W frequency comb at 2.8–4.8 μm," Opt. Lett. **34**, 1330–1332 (2009).

23. J. Buldt, H. Stark, M. Müller, C. Grebing, C. Jauregui, and J. Limpert, "Gas-plasma-based generation of broadband terahertz radiation with 640 mW average power," Opt. Lett. **46**, 5256–5259 (2021).

24. O. H. Heckl, C. J. Saraceno, C. R. E. Baer, T. Südmeyer, Y. Y. Wang, Y. Cheng, F. Benabid, and U. Keller, "Temporal pulse compression in a xenon-filled Kagome-type hollow-core photonic crystal fiber at high average power," Opt. Express **19**, 19142–19149 (2011).

25. C. J. Saraceno, O. H. Heckl, C. R. E. Baer, T. Südmeyer, and U. Keller, "Pulse compression of a high-power thin disk laser using rod-type fiber amplifiers," Opt. Express **19**, 1395–1407 (2011).

26. G. Cerullo and S. De Silvestri, "Ultrafast optical parametric amplifiers," Rev. Sci. Instrum. **74**, 1–18 (2003).

27. C. Manzoni and G. Cerullo, "Design criteria for ultrafast optical parametric amplifiers," J. Opt. **18**, 103501 (2016).

28. M. Brinkmann, T. Hellwig, and C. Fallnich, "Optical parametric chirped pulse oscillation," Opt. Express **25**, 12884–12895 (2017).

29. R. Das, S. C. Kumar, G. K. Samanta, and M. Ebrahim-Zadeh, "Broadband, high-power, continuous-wave, mid-infrared source using extended phase-matching bandwidth in MgO:PPLN," Opt. Lett. **34**, 3836–3838 (2009).

30. C. F. O'Donnell, S. C. Kumar, and M. Ebrahim-Zadeh, "Enhancement of efficiency in femtosecond optical parametric oscillators using group-velocity-matching in long nonlinear crystals," APL Photon. **4**, 050801 (2019).

31. A. Dubietis, G. Jonušauskas, and A. Piskarskas, "Powerful femtosecond pulse generation by chirped and stretched pulse parametric amplification in BBO crystal," Opt. Commun. **88**, 437–440 (1992).

32. G. Andriukaitis, T. Balčiūnas, S. Ališauskas, A. Pugžlys, A. Baltuška, T. Popmintchev, M.-C. Chen, M. M. Murnane, and H. C. Kapteyn, "90 GW peak power few-cycle mid-infrared pulses from an optical parametric amplifier," Opt. Lett. **36**, 2755–2757 (2011).

33. Y. Liu, W. Li, D. Luo, D. Bai, C. Wang, and H. Zeng, "Generation of 33 fs 935 W average power pulses from a third-order dispersion managed self-similar fiber amplifier," Opt. Express **24**, 10939–10945 (2016).

34. Y. Zhang, R. Chen, H. Huang, Y. Liu, H. Teng, S. Fang, W. Liu, F. Kaertner, J. Wang, G. Chang, and Z. Wei, "High-power pre-chirp managed amplification of circularly polarized pulses using high-dispersion chirped mirrors as a compressor," OSA Contin. **3**, 1988–1998 (2020).

35. A. Ruehl, A. Marcinkevicius, M. E. Fermann, and I. Hartl, "80 W, 120 fs Yb-fiber frequency comb," Opt. Lett. **35**, 3015–3017 (2010).

36. G. Barbiero, H. Wang, M. Graßl, S. Gröbmeyer, D. Kimbaras, M. Neuhaus, V. Pervak, T. Nubbemeyer, H. Fattahi, and M. F. Kling, "Efficient nonlinear compression of a thin-disk oscillator to 85 fs at 55 W average power," Opt. Lett. **46**, 5304–5307 (2021).

37. C. Grebing, M. Müller, J. Buldt, H. Stark, and J. Limpert, "Kilowatt-average-power compression of millijoule pulses in a gas-filled multi-pass cell," Opt. Lett. **45**, 6250–6253 (2021).

38. M. Müller, J. Buldt, H. Stark, C. Grebing, and J. Limpert, "Multipass cell for high-power few-cycle compression," Opt. Lett. **46**, 2678–2681 (2021).

39. J. Rothhardt, S. Hädrich, H. Carstens, N. Herrick, S. Demmler, J. Limpert, and A. Tünnermann, "1 MHz repetition rate hollow fiber pulse compression to sub-100-fs duration at 100 W average power," Opt. Lett. **36**, 4605–4607 (2011).

40. R. Klas, A. Kirsche, M. Gebhardt, J. Buldt, H. Stark, S. Hädrich, J. Rothhardt, and J. Limpert, "Ultra-short-pulse high-average-power megahertz-repetition-rate coherent extreme-ultraviolet light source," PhotoniX **2**, 4 (2021).

41. A.-L. Viotti, M. Seidel, E. Escoto, S. Rajhans, W. P. Leemans, I. Hartl, and C. M. Heyl, "Multi-pass cells for post-compression of ultrashort laser pulses," Optica **9**, 197–216 (2022).

42. T. Nagy, P. Simon, and L. Veisz, "High-energy few-cycle pulses: post-compression techniques," Adv. Phys. X **6**, 1845795 (2021).

43. P. Gierschke, C. Jauregui, T. Gottschall, and J. Limpert, "Relative amplitude noise transfer function of an Yb^{3+}-doped fiber amplifier chain," Opt. Express **27**, 17041–17050 (2019).

44. A. S. Mayer, W. Grosinger, J. Fellinger, G. Winkler, L. W. Perner, S. Droste, S. H. Salman, C. Li, C. M. Heyl, I. Hartl, and O. H. Heckl, "Flexible all-PM NALM Yb:fiber laser design for frequency comb applications: operation regimes and their noise properties," Opt. Express **28**, 18946–18968 (2020).

45. I. L. Budunoğlu, T. Bagci, C. Ülgüdür, K. Gürel, and F. O. Ilday, "Intensity noise of mode-locked Yb-doped fiber lasers," Opt. Lett. **34**, 2516–2518 (2009).

46. J. Fellinger, G. Winkler, A. S. Mayer, L. R. Steidle, and O. H. Heckl, "Tunable dual-color operation of Yb:fiber laser via mechanical spectral subdivision," Opt. Express **27**, 5478–5486 (2019).

47. J. Fellinger, A. S. Mayer, G. Winkler, W. Grosinger, G.-W. Truong, S. Droste, C. Li, C. M. Heyl, I. Hartl, and O. H. Heckl, "Tunable dual-comb from an all-polarization- maintaining single-cavity dual-color Yb:fiber laser," Opt. Express **27**, 28062–28074 (2019).

48. J. Buckley, A. Chong, S. Zhou, W. Renninger, and F. W. Wise, "Stabilization of high-energy femtosecond ytterbium fiber lasers by use of a frequency filter," J. Opt. Soc. Am. B **24**, 1803–1806 (2007).

49. P. Qin, Y. Song, H. Kim, J. Shin, D. Kwon, M. Hu, C. Wang, and J. Kim, "Reduction of timing jitter and intensity noise in normal-dispersion passively mode-locked fiber lasers by narrow band-pass filtering," Opt. Express **22**, 28276–28283 (2014).

50. M. E. Fermann, L. Turi, M. Hofer, F. Haberl, and A. J. Schmidt, "Additive-pulse-compression mode locking of a neodymium fiber laser," Opt. Lett. **16**, 244–258 (1991).

51. L. Nugent-Glandorf, T. A. Johnson, Y. Kobayashi, and S. A. Diddams, "Impact of dispersion on amplitude and frequency noise in a Yb-fiber laser comb," Opt. Lett. **36**, 1578–1580 (2011).

52. A. Pugžlys, G. Andriukaitis, A. Baltuška, L. Su, J. Xu, H. Li, R. Li, W. J. Lai, P. B. Phua, R. Danielius, and S. Ališauskas, "Multi-mJ, 200-fs, cw-pumped, cryogenically cooled, Yb,Na:CaF$_2$ amplifier," Opt. Lett. **34**, 2075–2077 (2009).

53. M. M. Jørgensen, S. R. Petersen, M. Laurila, J. Lægsgaard, and T. T. Alkeskjold, "Optimizing single mode robustness of the distributed modal filtering rod fiber amplifier," Opt. Express **20**, 7263–7273 (2012).

54. M. Laurila, T. T. Alkeskjold, J. Broeng, and J. Lægsgaard, "Distributed mode filtering rod fiber amplifier with improved mode stability," Opt. Express **20**, 5742–5753 (2012).

55. G. Feldhaus and A. Roth, "A 1 MHz to 50 GHz direct down-conversion phase noise analyzer with cross-correlation," in *European Frequency and Time Forum (EFTF)* (2016), pp. 2–5.

56. H. Tünnermann, J. Neumann, D. Kracht, and P. Weßels, "Gain dynamics and refractive index changes in fiber amplifiers: a frequency domain approach," Opt. Express **20**, 13539–13550 (2012).